Article | Open Access

Energy Materials

Dong *et al. Energy Mater.* **2026**, *6*, 600055 **DOI:**10.20517/energymater.2026.35

"One stone-two birds": reviving waste-activated carbon for stable polysulfide shuttle-free room-temperature Na-S batteries

Chunwei Dong[1], Zhihua Han[1], Zhijiang Su[1], Yang Dong[1], Quanbin Chen[1], Guofeng He[1], Xiaojie Sun[1], Nannan Zhang[1,*], Qing Jiang[2,*], Xiangjun Pu[3,*]

Keywords:
Sodium-sulfur batteries, shuttle effect, waste activated carbon, functionalized separator

Citation: Dong, C.; Han, Z.; Su, Z.; Dong, Y.; Chen, Q.; He, G.; Sun, X.; Zhang, N.; Jiang, Q.; Pu, X. "One stone-two birds": reviving waste-activated carbon for stable polysulfide shuttle-free room-temperature Na-S batteries. *Energy Mater.* **2026**, *6*, 600055. https://dx.doi.org/10.20517/energymater.2026.35

Received: 17 Mar 2026
Accepted: 30 Apr 2026
Published: 29 May 2026

Academic Editor:
Jung Ho Kim
Copy Editor:
Ping Zhang
Production Editor:
Ping Zhang

Abstract

Room-temperature sodium-sulfur batteries offer great potential for large-scale energy storage due to their high energy density, remarkable affordability, and abundant resources. However, its practical application is significantly hampered by the shuttle effect of Na_2S_x (x = 1, 2, 4, 6), which leads to the irreversible loss of active sulfur species and parasitic reactions, resulting in low reversible capacity and rapid capacity degradation. In this study, we propose a sustainable approach that utilizes waste activated carbon to transform the conventional glass-fiber separator into a functional separator. The functional separator effectively mitigates the polysulfide shuttle effect through the synergistic effects of physical adsorption and chemical bonding, as supported by both experimental observations and density functional theory calculations. Consequently, the cell utilizing the functionalized separator delivers an enhanced capacity of 698.2 mAh g^{-1} and superior stability (degradation rate 0.08%/cycle during 260 cycles). This design represents a

[1]National Institute of Clean-and-Low-Carbon Energy, Beijing 102209, China.
[2]Key Laboratory of Automobile Materials, Ministry of Education, School of Materials Science and Engineering, Jilin University, Changchun 130022, Jilin, China.
[3]Institute for Carbon Neutrality, Wuhan University, Wuhan 430072, Hubei, China.

[*]**Correspondence to:** Dr. Nannan Zhang, National Institute of Clean-and-Low-Carbon Energy, Beijing 102209, China. E-mail: 20099643@ceic.com; Prof. Qing Jiang, Key Laboratory of Automobile Materials, Ministry of Education, School of Materials Science and Engineering, Jilin University, Changchun 130022, Jilin, China. E-mail: jiangq@jlu.edu.cn; Dr. Xiangjun Pu, Institute for Carbon Neutrality, Wuhan University, Wuhan 430072, Hubei, China. E-mail: joy_pu@whu.edu.cn

promising pathway toward sustainable, room-temperature sodium-sulfur batteries, while also introducing an innovative method for the repurposing of industrial waste.

INTRODUCTION

Rechargeable batteries represent a critical enabler of the low-carbon economy, with annual production capacity projected to expand tenfold by 2030[1]. Lithium-ion batteries (LIBs), while studied extensively, may prove insufficient for this escalating demand due to the inherent scarcity and geopolitical concentration of lithium reserves[2-6]. Alternatively, room-temperature sodium-sulfur (RT Na-S) batteries are therefore garnering significant interests, owing to the impressive energy density (1,274 Wh kg^{-1}), remarkable affordability, and earth-abundant nature of sodium and sulfur[7-11]. However, practical deployment this technology faces critical challenges, notably the detrimental self-discharge issue[12] induced by the severe shuttle effect of sodium polysulfides (Na_2S_x, x = 1, 2, 4, 6)[13-15]. In specific, these soluble intermediates would dissolve and diffuse between two electrodes, leading to irreversible active material loss, low Coulombic efficiency, and rapid capacity degradation[16-18]. Activated carbon (AC) featuring large specific surface area, excellent porosity, and chemical tunability, has been widely applied in industrial fields including gas purification, water treatment, and electrochemical energy storage[19]. Global consumption of activated carbon exceeds 2 million tons annually[20], with increasing demand driven by environmental regulations and energy applications. Consequently, large amounts of spent or waste activated carbon (WAC) are generated each year[21]. Currently, the primary treatment strategies for waste AC include landfill disposal, thermal regeneration, and incineration-all of which suffer from high energy consumption, secondary pollution, or low recovery efficiency [Figure 1][22-25]. Effective reutilization of WAC remains a challenge that has not been sufficiently studied in the context of sustainable material cycling.

To mitigate the shuttle effect, a variety of strategies have been proposed. These include the design of polar host materials to trap polysulfides[26], the development of catalytic interlayers to accelerate redox kinetics[27], and the functionalization of separators to act as physical and chemical barriers[28]. In particular, separator modification stands out as a facile and scalable solution, capable of directly addressing polysulfide migration without significantly altering the battery architecture. Recent studies have introduced metal oxides, doped carbons, and metal-organic framework (MOF)-based coatings on commercial separators to improve electrochemical stability. For example, modifying glass fiber (GF) separators with Fe^{3+}/polyacrylamide nanospheres[29] and Al_2O_3-Nafion[30]. However, these materials often involve high-cost synthesis or limited sustainability.

In this contribution, we report a sustainable separator engineering strategy by repurposing nitrogen-doped activated carbon (N-AC) as a functional coating layer on commercial GF separator [Figure 1]. The N-AC provides a high surface area and abundant nitrogen/oxygen functionalities, enabling strong physical adsorption and chemical interaction with all Na_2S_x (x = 1, 2, 4, 6) species. The functionalized separator exhibits excellent polysulfide-blocking capability, validated by experiments and calculations. As a result, the cell with functional separator delivers outstanding long-term cycling stability, while simultaneously addressing the environmental challenge of WAC disposal, conceptualizing a “one stone-two birds” design.

EXPERIMENTAL

Nitrogen doping of waste activated carbon

The waste-activated carbon (sourced from Ningxia Coal Industry Co., Ltd., China Energy and Investment Group) was treated in a tube furnace at 800 °C for 5 h under a continuous argon flow to remove impurities. After cooling to room temperature, the resulting product was dispersed in 0.2 M hydrochloric acid and magnetically stirred for 30 min to unclog/clear pore channels and increase the specific surface area. The

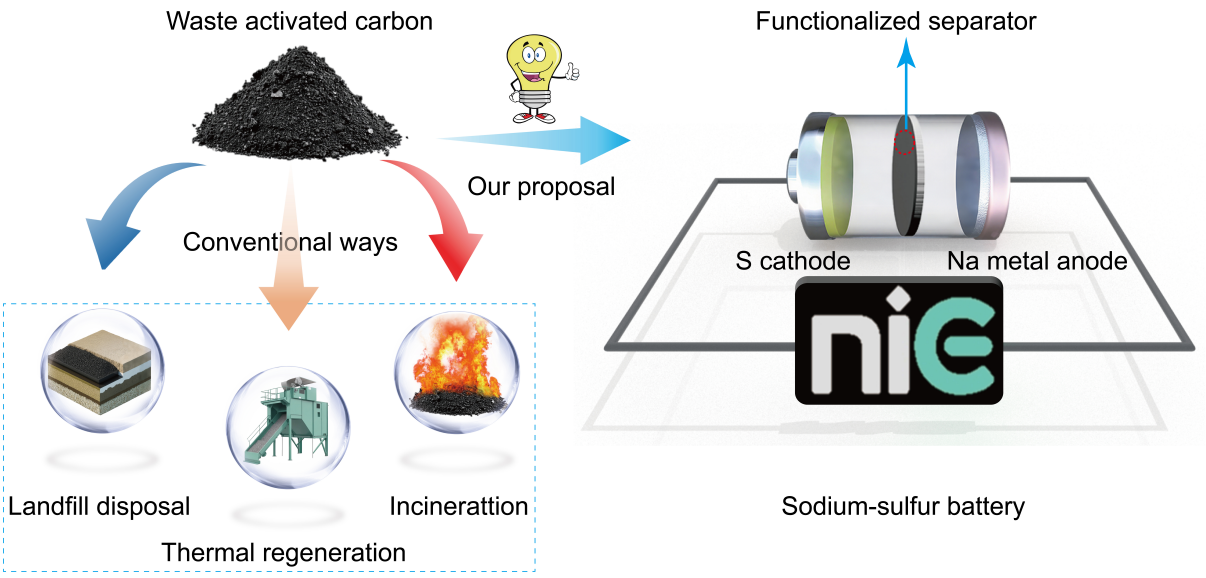

Figure 1. Schematic illustration of conventional waste activated carbon treatment methods versus the approach employed in this study.

mixture was then centrifuged, washed repeatedly with deionized water, and dried in a vacuum oven at 60 °C for 10 h to obtain porous carbon. In the following step, melamine and the prepared porous carbon (mass ratio 5:1) were placed separately into two crucibles and heated to 850 °C for 3 h in an Ar flow, then cooled naturally to room temperature, yielding N-AC.

Preparation of functional separator

The functional separator was obtained by a conventional filtration process. In specific, a suspension of 9 mg N-AC and 1 mg of graphene oxide in 100 mL of ethanol was sonicated for 30 min at room temperature. The resulting suspension was then poured into a Buchner funnel, using a GF separator (Whatman GF/C, diameter 90 mm, 100 sheets/box) as the filter. After filtration, the glass fiber separator was removed and dried under vacuum at 60 °C for 24 h, yielding the functional activated carbon modified GF separator (GF@N-AC).

Electrochemical measurements

The carbon-black sulfur (CB/S) composite was mixed with Super P and polyvinylidene fluoride (PVDF) in a mass ratio of 8:1:1 in N-methyl-2-pyrrolidone (NMP) solvent to make a slurry. The slurry was then uniformly casted onto aluminum foil, and dried at 60 °C for 12 h to punch into electrodes. To evaluate the effectiveness of the functionalized separator, the CR2032 coin cell is assembled in an argon-filled glovebox (O_2 and H_2O lower than 0.1 ppm). CR2032 coin cells were assembled using a CB/S cathode, a sodium metal anode, either a pristine glass fiber separator or a nitrogen-doped activated carbon-coated glass fiber separator, and an electrolyte of 1 mol/L sodium perchlorate in ethylene carbonate/diethyl carbonate (1:1, v/v). The sulfur loading of the cathode is ~0.86 mg cm^{-2}. All coin cells were tested on CT2001A Battery Tester. (Wuhan Land Electronics Co., Ltd, China).

Characterization

Thermogravimetric analysis (TGA): TGA was carried out under N_2 flow from room temperature to 800 °C at a rate of 10 °C min^{-1} using an STA 449C thermogravimetric analyzer, which is located at the Materials Characterization Center of the National Institute of Clean-and-Low-Carbon Energy.

X-ray diffraction (XRD): The pristine sample was measured in powder form. All patterns were recorded on Bruker D8 ADVANCE X-ray powder diffractometer utilizing Cu Kα radiation (λ = 0.15418 nm, 40 kV, 40 mA).

Raman spectroscopy: The samples for Raman spectroscopy were prepared in the same way as the XRD analysis. Raman spectroscopic analysis was performed with a laser confocal Raman spectrometer (RAMAN, Horiba Jobin Yvon, LabRam HR-800), located in the Materials Characterization Center of National Institute of Clean-and-Low-Carbon Energy, utilizing an excitation wavelength of 532 nm.

X-ray photoelectron spectroscopy (XPS): The samples for XPS measurement were prepared in the same way as the Raman spectroscopy analysis. XPS measurements were carried out with ESCALab250Xi located in the Materials Characterization Center of National Institute of Clean-and-Low-Carbon Energy.

Scanning electron microscopy (SEM): The samples for SEM analysis were prepared as follows. The as-prepared functionalized separators were sectioned into squares with a side length of 2 mm using a precision disc cutter. The samples were mounted onto a conductive specimen stub. All observations were performed on FEI Nova NanoSEM 450 scanning electron microscope in National Institute of Clean-and-Low-Carbon Energy.

Brunauer-Emmett-Teller (BET): Nitrogen adsorption/desorption isotherms at 77 K were obtained on ASAP 2020 surface area and porosity analyzer (Micromeritics Instrument Corporation) located in National Institute of Clean-and-Low-Carbon Energy".

Density functional theory calculations

In this work, density functional theory calculations were carried out using the Vienna Ab initio Simulation Package (VASP, version 5.4.4) with the projector augmented wave (PAW) method[31-34]. The exchange-correlation energy was described using the Perdew-Burke-Ernzerhof (PBE) functional within the generalized gradient approximation[35], and van der Waals interactions were accounted for using Grimme's density functional theory (DFT)-D3 method[36]. The energy cutoff for the plane-wave basis sets was set to 400 eV, and a 3 × 3 × 1 gamma-centered k-point grid was used to sample the Brillouin zone. The geometry optimization and self-consistent field convergence criteria were set to 0.03 eV $Å^{-1}$ and 10^{-5} eV, respectively. All supercells include a vacuum layer of 15 Å. The microstructure of activated carbon consists of disordered stacked sp^2-hybridized carbon layers, exhibiting significant local aromatic character. Its fundamental structural units share identical chemical bonding environments and electronic structural features with graphene, making graphene an ideal simplified model. By introducing defects such as vacancies and heteroatom doping, the graphene model can effectively simulate the chemical properties of the activated carbon surface. Thus, in this study, a graphene-based model is employed to investigate the microscopic mechanisms of polysulfide transformation on activated carbon. The adsorption energy (ΔE_{ad}) of sodium polysulfides (SPSs) on the substrate was calculated by using $\Delta E_{ad} = \Delta E_{sys} - (\Delta E_{Na2Sx} + \Delta E_{surf})$, where ΔE_{sys}, ΔE_{Na2Sx}, and ΔE_{surf} are the total energy of the adsorbed system, the energy of the adsorbate in a vacuum, and the energy of the optimized surface, respectively. In this work, the adsorption energy (ΔE_{ad}) is defined as $\Delta E_{ad} = E_{sys} - (E_{Na2Sx} + E_{surf})$. Therefore, a negative ΔE_{ad} value indicates an exothermic and stable adsorption process. For N-doped carbon, three common configurations were considered, namely graphitic N, pyridinic N, and pyrrolic N.

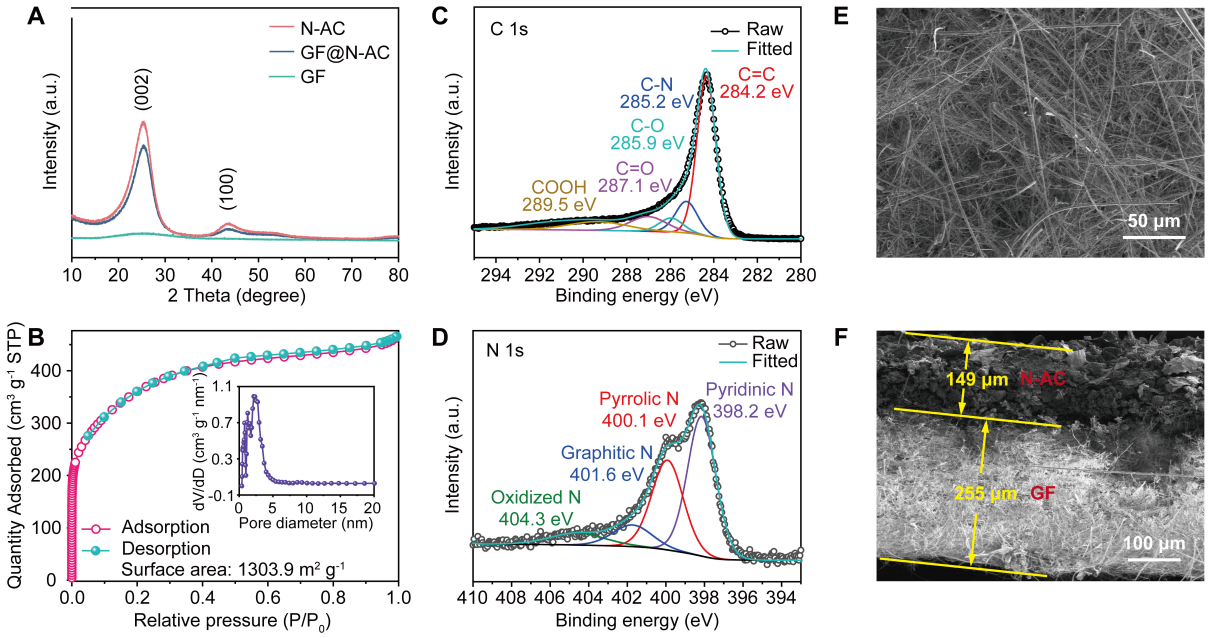

Figure 2. Derivation and characterization of N-AC and functionalized glassfiber separators (GF@N-AC). (A) XRD patterns of N-AC, GF@N-AC and GF; (B) Nitrogen adsorption/desorption curves of N-AC sample [the inset shows the pore distribution calculated by Barret-Joyner-Halenda (BJH) model]; Deconvolution of high-resolution XPS spectra for C 1s (C) and N 1s (D) of N-AC; (E and F) SEM images of the bare GF separator (E) and cross-sectional image of the functionalized separator (F). XRD: X-ray diffraction; N-AC: nitrogen-doped activated carbon; GF: glass fiber; XPS: X-ray photoelectron spectroscopy; SEM: scanning electron microscopy; STP: standard temperature and pressure.

RESULTS AND DISCUSSION

Derivation and characterization of the functionalized glassfiber separators

The detailed preparation process is displayed in Supplementary Figure 1, where the waste N-AC was feasibly coated on the glassfiber separators by a consecutive dispersion-filtration operation. The crystal phase of N-AC, GF@N-AC and GF was investigated by XRD. Displayed in Figure 2A, the pristine GF separator exhibits an amorphous character, whereas N-AC and GF@N-AC display peaks at 25.5° and 43.6°, corresponding to the (002) and (100) planes, respectively, indicating that the structure of N-AC is preserved after coating onto the GF fibers. Furthermore, the XRD pattern of the CB/S cathode is presented in Supplementary Figure 2, confirming the successful preparation of the composite material. Figure 2B presents the nitrogen adsorption-desorption isotherms and pore size distribution of the N-AC. It shows a specific area of 1303.9 $m^2 g^{-1}$ with the pore size centered at 2.21 nm, calculated by Barret-Joyner-Halenda (BJH) model. The Raman spectroscopy [Supplementary Figure 3] reveals distinct D and G bands at 1,336 and 1,588 cm^{-1}, respectively, with an intensity ratio (ID/IG) of 1.25, indicating a relatively high degree of graphitization[37-40]. Further insights into the surface chemistry of N-AC are provided by XPS analysis. As shown in Supplementary Figure 4, the XPS survey of the N-AC shows the presence of the carbon and nitrogen, corresponding element contents of 91.89% and 8.11%, respectively. The high-resolution C 1s spectrum [Figure 2C] can be deconvoluted into five distinct peaks at 284.2, 285.2, 285.9, 287.1, and 289.5 eV, ascribing to C=C, C-N, C-O, C=O, and COOH, respectively[41,42]. Whereas the N 1s spectrum can be split into four types of nitrogen species-pyridinic (41.1%), pyrrolic (31.3%), and graphitic (12.7%) and oxidized (14.9%) nitrogen [Figure 2D and Supplementary Table 1]. These oxygen- and nitrogen-containing groups enhance the chemical affinity of the material for polysulfides, which we will present below.

The pristine separator features abundant pores [Figure 2E], enabling efficient sodium-ion transport. However, this configuration allows polysulfide species to migrate freely to the anode, triggering the shuttle effect, which results in active material loss and deteriorates electrochemical performance. In this regard, we

proposed to leverage the GF separator with nitrogen-doped activated carbon [Supplementary Figures 5 and 6]. Cross-sectional SEM imaging confirms that the coating thickness of the porous N-AC [Figure 2F] is approximately 149 μm. The mechanical performance of the GF@N-AC separator was assessed by bending tests together with post-bending structural characterization. As shown in Supplementary Figure 7, the separator maintained its structural integrity during both forward and backward bending without visible cracking, indicating excellent flexibility and strong adhesion between the N-AC coating and the GF substrate. SEM images further show that the coating remained uniformly attached to the GF separator without noticeable delamination or peeling after bending [Supplementary Figure 8]. In addition, the corresponding energy-dispersive spectroscopy (EDS) maps exhibit a uniform elemental distribution similar to that before bending [Supplementary Figure 9], confirming that the coating layer remained well preserved after mechanical deformation. These results confirm the superior mechanical durability of the modified separator and the strong bonding between the coating layer and the separator substrate.

For a preliminary analysis of the feasibility of GF@N-AC for room-temperature Na-S batteries, the ionic conductivity was assessed [Supplementary Figure 10]. As a result, the ionic conductivity of the GF@N-AC separator is calculated to be 3.1 mS cm^{-1}, higher that of the GF separator (1.6 mS cm^{-1}). Hence the modification of commercial GF separator with the porous N-AC could alleviate the side shuttle reactions and improve Na^+ ions diffusion.

Inhibiting capability of functional separator against polysulfide shuttle

The schematic illustrations of Na-S batteries employing pristine and functional separators are comparatively shown in Figures 3A and B. A lingering challenge for Na-S batteries is the shuttle effect, which arises when soluble polysulfides generated during cycling diffuse through the electrolyte and continuously migrate between the electrodes. This leads to the irreversible loss of active sulfur species, severely compromising the overall electrochemical performance. The pristine GF separator with abundant micron-sized pores, allows not only the transport of sodium ions but also the free detrimental passage of polysulfides. In contrast, the functionalized separator-featuring a high surface area and nitrogen doping-effectively traps polysulfides through physical adsorption and chemical interactions, as analyzed by the leakage experiment in H-type cell. In this scenario, sodium hexasulfide (Na_2S_6) solution was placed on the left chamber, while pure tetraethylene glycol dimethyl ether (TEGDME) was added to the right side. The two chambers separated by either a pristine or a functional separator were placed at room temperature. Consequently, the pristine separator allows substantial migration of polysulfides after 12 h [Figure 3C]. In contrast, the H-cell equipped with the functionalized separator remained clear and transparent, confirming its superior blocking capability against polysulfide shuttle [Figure 3D]. Furthermore, we also evaluated the overall performance of GF@N-AC and GF separators when used in a full Na-S battery. As shown in Supplementary Figure 11, the GF@N-AC based cell exhibits smaller R_s (1.94-2.48 Ω) and R_{ct} (42.10-42.91 Ω) during the whole discharge process, demonstrating a faster electron/ion transport in the GF@N-AC based cell, whereas the GF-separator-based cells have higher R_s (5.52-5.89 Ω) and R_{ct} (216.3-274.5 Ω). This indicates that the functionalized separator prominently improves the internal sluggish kinetics caused by soluble sodium polysulfides, thereby promoting Na^+ transport rate.

Inhibition mechanism of sodium polysulfide shuttle by experimental study and theoretical calculation

To investigate the inhibitory mechanism of activated carbon-functionalized separators against SPSs, we separately introduced 0.1 g of N-AC into the base solution (0.5 M Na_2S_6 in TEGDME), as illustrated in Figure 4A. consequently, the upper section of the solution exhibited significant clarification after 6 hours, demonstrating the effective adsorption capability of N-AC towards Na_2S_6 polysulfides.

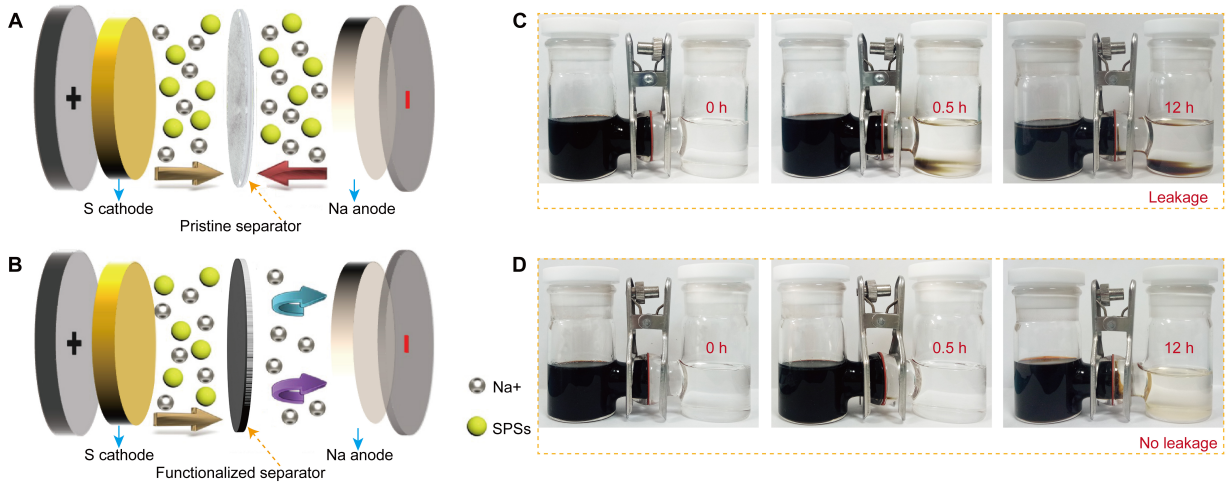

Figure 3. Evaluation of sodium polysulfide shuttle suppression capability. Schematic diagrams of the pristine (A) and functionalized separator (B) within the Na-S batteries; Polysulfide shuttle measurements with pristine GF (C) and wasted carbon functionalized separators (D) at 0, 0.5 and 12 h. (C and D were photographed by the author, without any copyright concerns). GF: Glass fiber.

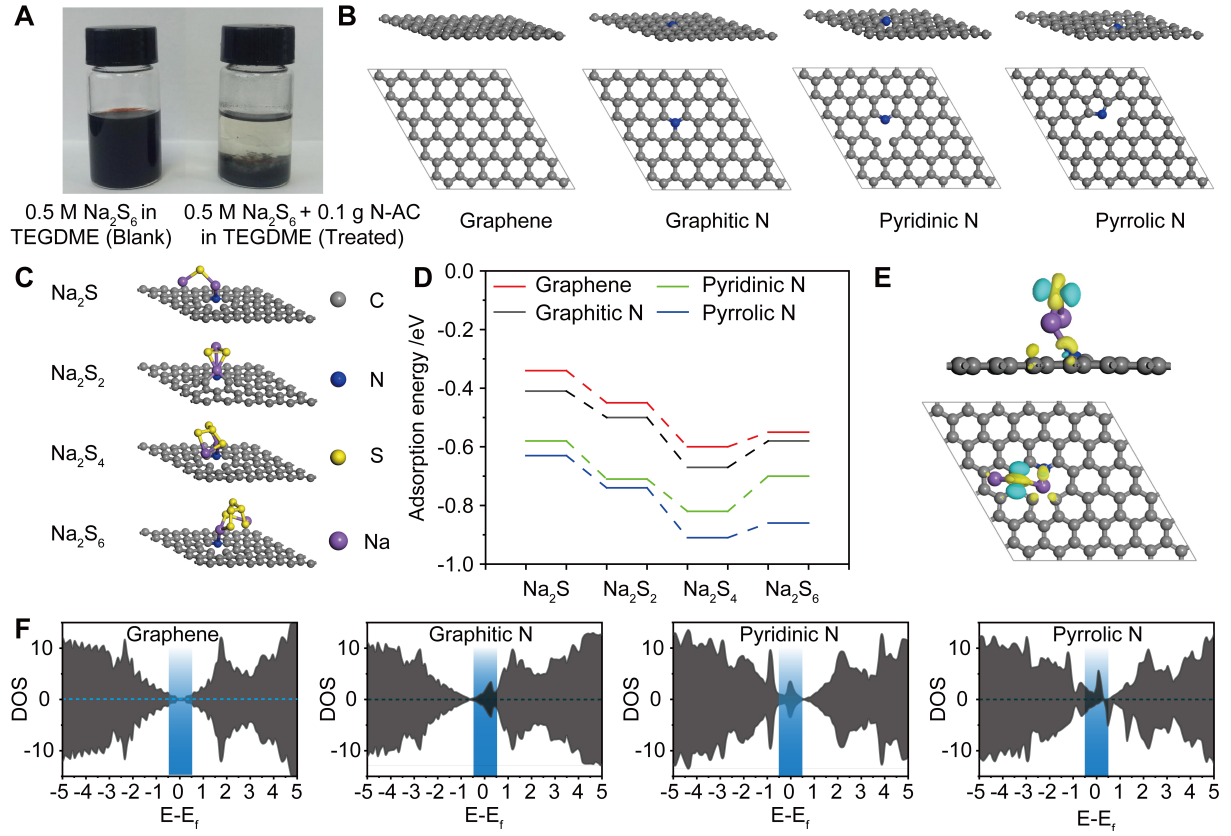

Figure 4. Polysulfide adsorption effects studied by experiment and DFT calculations. (A) Polysulfide adsorption effect in the blank and N-AC added electrolytes. (A was photographed by the author, without any copyright concerns); (B) The geometries of perfect graphene and defect graphene with graphitic N, pyridinic N, and pyrrolic N; Configurations of Na_2S_x (x = 1, 2, 4, 6) adsorbed on pyridinic N-doped graphene layers (C) with annotation of C (gray), N (blue), S (yellow), Na (purple), and their corresponding adsorption energy (D); (E) The charge density difference of the short-chain Na_2S/graphene. Where yellow- and blue-distribution correspond charge accumulation and depletion, respectively; (F) The DOS of graphene and graphene doped with graphitic N, pyridinic N, and pyrrolic N. DOS: Density of states; TEGDME: tetraethylene glycol dimethyl ether; DFT: density functional theory.

To gain deeper insights into the interaction mechanisms between all sodium polysulfides Na_2S_x (x = 1, 2, 4, 6) and nitrogen-doped activated carbon, we systematically performed DFT calculations. Given the structural complexity of amorphous activated carbon, a simplified graphene-based model system was adopted [Figure 4B], which is a well-accepted method to study activated carbon properties[43]. With pyridinic nitrogen-doped graphene as the representative, Figure 4C and Supplementary Figure 12 illustrate the optimized adsorption configurations of Na_2S_x species[44]. Notably, the DFT results reveal that the interaction mechanism involves two key aspects: (1) the positively charged Na^+ ions form coordination with the electron-rich nitrogen sites, and (2) the electron-rich sulfur atoms (S_x^{2-}) preferentially orient toward the vacuum region. DFT calculations also reveal a continuous interaction between other sodium polysulfides (Na_2S, Na_2S_2, Na_2S_4) and various nitrogen-doped graphene surfaces [Figure 4D][45,46]. In specific, pyridinic- and pyrrolic-N doped graphene demonstrate substantially lower adsorption energies for Na_2S_x, especially for the short-chain polysulfides (Na_2S, Na_2S_2) due to pronounced electron transfer [Figure 4E][47]. The detailed adsorption energy values are summarized in Supplementary Table 2. Furthermore, density of states (DOS) analysis [Figure 4F] confirms that nitrogen doping introduces abundant electronic states near the Fermi level, facilitating efficient electron transport during electrochemical processes[48]. In brief, defective graphene layers within activated carbon reveal strong adsorption capability towards all polysulfides Na_2S_x (x = 1, 2, 4, 6), contributing to inhibite shuttle effect in Na-S batteries.

Electrochemical performance of RT Na-S batteries with the functionalized separator

The above analyses underscore the capability of the functionalized separator in suppressing the shuttle effect of sodium polysulfides, thus we tentatively applied it to Na-S batteries. The thermogravimetric curve confims that the sulfur content in the cathode is approximately 70% [Supplementary Figure 13]. Figure 5A presents galvanostatic charge-discharge profiles of the cells with the functionalized separator. A significantly capacity of 985.5 mAh g^{-1} is reached initially with 662.5 mAh g^{-1} maintained after 100 cycles at 0.1 C (1 C = 1,672 mA g^{-1}). The charge-discharge curves are nearly overlapped from the 50th to 100th cycle with operating voltage around 1.3 V, demonstrating the excellent reversibility of the RT Na-S battery with the modified separator. Further insights into redox mechanisms can be inferred from the cyclic voltammetry (CV) curves (inset of Figure 5A): the two peaks at 1.48 and 0.98 V are relevant to the transition from solid sulfur to dissolved liquid long-chain Na_2S_x ($4< x \leq 8$), while the peak at 0.69 V corresponds to the long-chain polysulfides to insoluble short-chain polysulfides (Na_2S_2 and Na_2S). Subsequently, two peaks in the recharging process arise from the oxidation of polysulfides to solid sulfur reversibly. Compared to GF separator, CV curves measured from GF@N-AC separator overlapped, implying high reaction reversibility. The CV curves of cells based on GF@N-AC separator displayed a smaller polarization than GF separator (inset of Figure 5A and Supplementary Figure 14). As displayed in the primary comparative cycling measurements [Figure 5B], the cell employing the functionalized separator retains 67.3% capacity after 100 cycles. In contrast, the cell using the pristine separator delivered a low capacity of 590.2 mAh g^{-1}, which rapidly declined to only 285.6 mAh g^{-1} after merely 10 cycles. However, compared to the moderate thickness of N-AC (149 μm), the cell with increased thickness coating (192 μm) shows worse cycling (rapidly drops to 605.3 mAh g^{-1} after only 10 cycles). Therefore, a moderate coating thickness is essential for alleviation of the shuttle effect of soluble sodium polysulfides, but over thick coating compromises the mechanical integrity and cycling stability.

Furthermore, Figure 5C depicts the rate performance of batteries. A highest discharge capacity of 660.4, 470.8 and 390.1 mAh g^{-1} (at 0.5, 1 and 2 C, comparatively) is achieved in the cell with the modified separator, while for the cell with the pristine separator, an inferior capacity of below 200 mAh g^{-1} can only be reached at 0.5 C. It is worthy note that the performance (regarding reversible capacity and rate capability) with separator modification strategy proposed in this work is competitive/superior to other previous strategies[49-57] [Figure 5D]. Supplementary Figure 15 shows the EIS spectra at open-circuit voltage (OCV) of

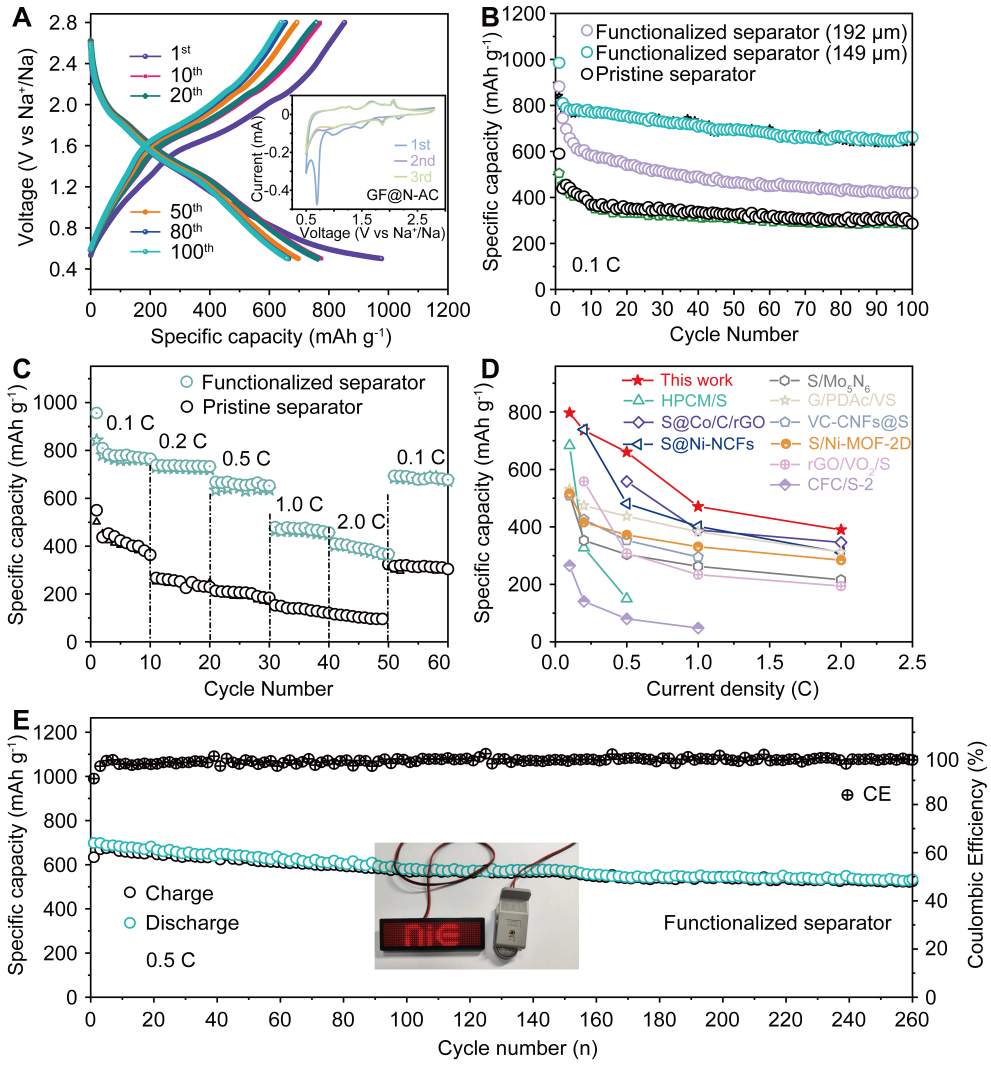

Figure 5. Comparative electrochemical performance of cells with the pristine and functionalized separators. (A) Typical galvanostatic charge-discharge curves of the cell with the functionalized separator (inset: CV curves at 0.1 mV s^{-1}). The primary comparative cycling stability at 0.1 C; (B) and the rate capabilities (C); (D) Performance comparison of separator modification strategy proposed in this work to other previous strategies; (E) Long-term cycling of the cell with functionalized separator at 0.5 C (inset: photographs of a coin cell lighting up a light-emitting diodes). (E was photographed by the author, without any copyright concerns). CV: Cyclic voltammetry; N-AC: nitrogen-doped activated carbon; CE: Coulombic efficiency.

room-temperature sodium-sulfur batteries employing a GF@N-AC separator. The corresponding charge-transfer resistance (R_{ct}) is 103.4 Ω, which is comparable to that of the cell with the pristine separator (120.6 Ω), indicating that the separator has a limited effect on interfacial charge transfer. The fitted data of the equivalent circuit for cells with GF@N-AC and GF separator are supplemented in Supplementary Table 3. Finally, the long-term cycling at higher 0.5 C rate was performed [Figure 5E]. The cell with the functional separator delivers an initial reversible capacity of 698.2 mAh g^{-1}, with 545.4 mAh g^{-1} remaining after 260 cycles. This corresponds to a minimal degradation rate of 0.08%/cycle and near 100% Coulombic efficiency, exceeding previous reports[58,59], by using a separator modified by waste activated carbon. Impressively, the assembled coin cell with GF@N-AC separators is able to light an electric-light emitting diode (LED) with the logo of "nice" (National Institute of Clean-and-Low-Carbon Energy) [inset of Figure 5E]. These results highlight the effectiveness of the functional separator in mitigating the polysulfide shuttle effect and ensuring stable Na-S battery operation.

Additionally, after 50 cycles, the modified separator retains an intact coating with negligible morphological change [Supplementary Figure 16]; Unlike the pure GF separator, which shows a rougher surface from electrolyte residue. EDS mapping analysis [Supplementary Figures 17 and 18] confirms sulfur presence only on the modified separator, indicating effective polysulfide adsorption. This is also consistent with the smoother sodium anode surface observed with the modified separator [Supplementary Figure 19], demonstrating its efficacy in suppressing shuttle and enhancing performance.

CONCLUSIONS

In this contribution, we have successfully proposed a sustainable and cost-effective strategy to enhance room-temperature sodium-sulfur (Na-S) batteries by repurposing N-AC to modify the commercial glass-fiber separator. The functionalized separator effectively suppresses the polysulfide shuttle through a combination of physical adsorption and chemical bonding, as confirmed by both experimental and theoretical analyses. Such modification significantly improves the initial capacity to 698.2 mAh g^{-1} and cycling stability (with a minimal degradation rate of 0.08% per cycle over 260 cycles). This strategy enhances the performance of Na-S batteries, and offers a promising solution to the environmental challenge posed by waste activated carbon, conceptualizing a "one stone-two birds" design.

DECLARATIONS

Authors' contributions

Methodology, formal analysis, and writing of the manuscript: Dong, C.
Data acquisition: Han, Z.
Data analysis and technical support: Su, Z.; Dong, Y.
Electrochemical performance measurements: Chen, Q.
Analysis and interpretation of the results: He, G.; Sun, X.
DFT calculations: Zhang, N.
supervised all aspects of this work: Pu, X.; Jiang, Q.
All authors participated in the discussion of the results and contributed to the final version of the manuscript.

Availability of data and materials

The data supporting our findings can be found in the Supplementary Materials.

AI and AI-assisted tools statement

Not applicable.

Financial support and sponsorship

The work described in this paper was supported by CHN Energy Investment Group (GJNY-25-104). Dr. Pu, X. acknowledges the Joint Postdoc Scheme from PolyU (1-45-35-YY4L), and the Brain Pool program (RS-2023-00273752) provided by the National Research Foundation (NRF) of South Korea.

Conflicts of interest

All authors declared that there are no conflicts of interest.

Ethical approval and consent to participate

Not applicable.

Consent for publication

Not applicable.

Supplementary Materials

Supplementary Materials

REFERENCES

1. Liu, Y.; Ma, S.; Rosebrock, M.; et al. Tungsten nanoparticles accelerate polysulfides conversion: a viable route toward stable room-temperature sodium-sulfur batteries. *Adv. Sci.* **2022**, *9*, 2105544. DOI
2. Yu, J.; Kim, D. K.; Oh, H. G.; Park, S. K.; Yoo, Y. N, P co-doped 3D porous carbon with self-assembled morphological control via template-free method for potassium-ion battery anodes. *Rare. Met.* **2024**, *43*, 4243-52. DOI
3. M Subramaniyam, C.; Kuhn, A.; González, E. G.; Guerrero-pérez, O.; Rodríguez-castellón, E.; García-alvarado, F. Cost effective synthesis of 3-dimensional V_4O_9: a promising high-capacity lithium cathode. *Catal. Today.* **2024**, *429*, 114507. DOI
4. Senguttuvan, P.; Lee, E.; Key, B.; Johnson, C. S. Synthesis, structural and electrochemical properties of V_4O_9 cathode for lithium batteries. *Front. Chem.* **2023**, *11*, 1161053. DOI
5. Mishra, Y.; Chattaraj, A.; Aljabali, A. A.; El-tanani, M.; Tambuwala, M. M.; Mishra, V. Graphene oxide-lithium-ion batteries: inauguration of an era in energy storage technology. *Clean. Energy.* **2024**, *8*, 194-205. DOI
6. Kong, J.; Su, Z.; Dong, C.; Chen, Q.; Pan, G. Overview of coals as carbon anode materials for sodium-ion batteries. *Clean. Energy.* **2024**, *8*, 197-218. DOI
7. Yao, G.; Li, Z.; Zhang, Y.; et al. Highly flexible carbon film implanted with single-atomic Zn-N_2 moiety for long-life sodium-sulfur batteries. *Adv. Funct. Mater.* **2023**, *34*, 2214353. DOI
8. Fan, Y.; Su, D.; Zheng, Y.; et al. Anionic MOF-derived Ni/$Ni_{1-x}O$ heterojunctions with electrochemically induced vacancy reconstruction: enabling high-rate and stable room-temperature Na-S batteries. *Adv. Energy. Mater.* **2025**, *16*, e04080. DOI
9. Xiao, T.; Fang, Z.; Ran, N.; et al. Amorphous/crystalline interwoven multipods with high Co/Ni activity for wide-temperature-range sodium-sulfur batteries. *Nat. Commun.* **2026**, *17*, 2333. DOI PubMed PMC
10. He, J.; Bhargav, A.; Shin, W.; Manthiram, A. Stable dendrite-free sodium-sulfur batteries enabled by a localized high-concentration electrolyte. *J. Am. Chem. Soc.* **2021**, *143*, 20241-8. DOI
11. Zhou, J.; Yang, Y.; Zhang, Y.; et al. Sulfur in amorphous silica for an advanced room-temperature sodium-sulfur battery. *Angew. Chem. Int. Ed.* **2021**, *60*, 10129-36. DOI
12. Pu, X.; Zheng, Y.; Qi, A.; et al. Understanding and illustrating the irreversible self-discharge in rechargeable batteries by the Evans Diagram. *Carbon. Neutraliz.* **2024**, *3*, 94-107. DOI
13. Ye, X.; Ruan, J.; Pang, Y.; et al. Enabling a stable room-temperature sodium-sulfur battery cathode by building heterostructures in multichannel carbon fibers. *ACS. Nano.* **2021**, *15*, 5639-48. DOI
14. Chen, S.; Liang, L.; Li, Y.; et al. Brain capillary-inspired self-assembled covalent organic framework membrane for sodium-sulfur battery separator. *Adv. Energy. Mater.* **2023**, *13*, 2204334. DOI
15. Wu, Y.; Huang, J.; Zhang, Z.; et al. Recent advances in functionalized separators for shuttle-free and dendrite-free lithium/sodium-sulfur batteries. *Energy. Mater.* **2025**, *5*, 500027. DOI
16. Xiong, Z.; Chen, S.; Guo, J.; et al. In situ observation of Na_2S growth: a step toward high-energy and safer room temperature sodium sulfur batteries. *Adv. Mater.* **2025**, *38*, e05966. DOI
17. Wang, Y. X.; Zhang, B.; Lai, W.; et al. Room-temperature sodium-sulfur batteries: a comprehensive review on research progress and cell chemistry. *Adv. Energy. Mater.* **2017**, *7*, 1602829. DOI
18. Zhou, F.; Wu, Q.; Meng, J.; Xu, J.; Cao, F. Rare-earth-based strategies for lithium-sulfur batteries: enhancing multi-electron conversion reaction kinetics. *Energy. Z.* **2025**, *1*. DOI
19. Devi, R.; Kumar, V.; Kumar, S.; et al. Recent advancement in biomass-derived activated carbon for waste water treatment, energy storage, and gas purification: a review. *J. Mater. Sci.* **2023**, *58*, 12119-42. DOI
20. Global demand for activated carbon to exceed two million metric tons in 2018. https://www.watertechonline.com/home/article/1554527/global-demand-for-activated-carbon-to-exceed-two-million-metric-tons-in-2018. (accessed 2026-05-18).
21. Li, C.; Zhao, X.; Pang, T.; Hu, N.; Zheng, T. Multiphysics simulation and optimization of microwave-assisted regeneration of spent activated carbon for enhanced energy efficiency. *Environ. Res.* **2025**, *285*, 122292. DOI
22. Chen, X.; Tian, Z.; Yang, Q.; et al. Cost-effective H_2O_2-regeneration of powdered activated carbon by isolated Fe sites. *Adv. Sci.* **2022**, *10*, 2204079. DOI PubMed PMC
23. Ayaz, M.; Shah, S. S.; Younas, M.; et al. Green synthesis of activated carbon from biomass waste of date palm seeds: a sustainable solution for energy storage and environmental impact. *J. Energy. Storage.* **2025**, *110*, 115291. DOI
24. Liu, Z.; Liu, L.; Fu, Y.; et al. In situ regeneration of phenol-saturated activated carbon fiber via an electro-permanganate process. *J. Water. Process. Eng.* **2025**, *72*, 107654. DOI

25. Sousa, É.; Rocha, L.; Jaria, G.; et al. Optimizing microwave-assisted production of waste-based activated carbons for the removal of antibiotics from water. *Sci. Total. Environ.* **2021**, *752*, 141662. DOI
26. Wang, P.; Sun, S.; Rui, X.; et al. Polar Electrocatalysts for preventing polysulfide migration and accelerating redox kinetics in room-temperature sodium-sulfur batteries. *Small. Methods.* **2023**, *7*, 2201728. DOI
27. Jin, F.; Wang, B.; Wang, J.; et al. Boosting electrochemical kinetics of S cathodes for room temperature Na/S batteries. *Matter* **2021**, *4*, 1768-800. DOI
28. Eng, A. Y. S.; Kumar, V.; Zhang, Y.; et al. Room-temperature sodium-sulfur batteries and beyond: realizing practical high energy systems through anode, cathode, and electrolyte engineering. *Adv. Energy. Mater.* **2021**, *11*, 2003493. DOI
29. Mei, T.; Li, X.; Lin, X.; Bai, L.; Xu, M.; Qi, Y. Cobalt catalytic regulation engineering in room-temperature sodium-sulfur batteries: facilitating rapid polysulfides conversion and delicate Na_2S nucleation. *Adv. Funct. Mater.* **2024**, *35*, 2418126. DOI
30. Ceylan Cengiz, E.; Erdol, Z.; Sakar, B.; et al. Investigation of the effect of using Al_2O_3-nafion barrier on room-temperature Na-S batteries. *J. Phys. Chem. C.* **2017**, *121*, 15120-6. DOI
31. Kresse, G.; Hafner, J. *Ab initio*molecular dynamics for liquid metals. *Phys. Rev. B.* **1993**, *47*, 558-61. DOI
32. Kresse, G.; Furthmüller, J. Efficiency of ab-initio total energy calculations for metals and semiconductors using a plane-wave basis set. *Comp. Mater. Sci.* **1996**, *6*, 15-50. DOI
33. Kresse, G.; Furthmüller, J. Efficient iterative schemes for*ab initio* total-energy calculations using a plane-wave basis set. *Phys. Rev. B.* **1996**, *54*, 11169-86. DOI
34. Kresse, G.; Joubert, D. From ultrasoft pseudopotentials to the projector augmented-wave method. *Phys. Rev. B.* **1999**, *59*, 1758-75. DOI
35. Perdew, J. P.; Burke, K.; Ernzerhof, M. Generalized gradient approximation made simple. *Phys. Rev. Lett.* **1996**, *77*, 3865-8. DOI
36. Grimme, S.; Antony, J.; Ehrlich, S.; Krieg, H. A consistent and accurate*ab initio*parametrization of density functional dispersion correction (DFT-D) for the 94 elements H-Pu. *J. Chem. Phys.* **2010**, *132*, 154104. DOI
37. Xiao, F.; Yang, X.; Wang, H.; et al. Covalent encapsulation of sulfur in a MOF-derived S, N-doped porous carbon host realized via the vapor-infiltration method results in enhanced sodium-sulfur battery performance. *Adv. Energy. Mater.* **2020**, *10*, 2000931. DOI
38. He, S.; Yang, J.; Liu, S.; et al. Asymmetric N-coordinated iron single-atom catalysts supported on graphitic carbon for polysulfide conversion in lithium-sulfur batteries. *Chem. Eng. J.* **2023**, *454*, 140202. DOI
39. Zhang, M.; Mu, J.; Li, Y.; et al. Propelling polysulfide redox by Fe_3C-FeN heterostructure@nitrogen-doped carbon framework towards high-efficiency Li-S batteries. *J. Energy. Chem.* **2023**, *78*, 105-14. DOI
40. Jing, W.; Tan, Q.; Duan, Y.; et al. Defect-rich single atom catalyst enhanced polysulfide conversion kinetics to upgrade performance of Li-S batteries. *Small* **2022**, *19*, 2204880. DOI
41. Saroha, R.; Lee, J. S.; Cho, S. W.; Cho, C.; Park, J.; Cho, J. S. Polysulfide barrier comprising bismuth selenide nanocrystals well anchored within N-doped carbon microspheres for stable Li-S batteries. *Energy. Mater.* **2025**, *5*, 500089. DOI
42. Lin, C.; Zhang, J.; Lim, Y. V.; et al. 3D hierarchical architectures of $CoSe_2$ nanoparticles embedded in rice-derived hard carbon for advanced sodium storage. *Carbon. Neutraliz.* **2022**, *1*, 224-32. DOI
43. Xiao, F.; Wang, H.; Xu, J.; et al. Generating short-chain sulfur suitable for efficient sodium-sulfur batteries via atomic copper sites on a N,O-codoped carbon composite. *Adv. Energy. Mater.* **2021**, *11*, 2100989. DOI
44. Zheng, F.; Zhang, Y.; Ding, G.; et al. Pentagon defects accelerating polysulfides conversion enabled high-performance sodium-sulfur batteries. *Adv. Funct. Mater.* **2023**, *34*, 2310598. DOI
45. Zhang, B.; Sheng, T.; Liu, Y.; et al. Atomic cobalt as an efficient electrocatalyst in sulfur cathodes for superior room-temperature sodium-sulfur batteries. *Nat. Commun.* **2018**, *9*, 4082. DOI
46. Yan, Z.; Xiao, J.; Lai, W.; et al. Nickel sulfide nanocrystals on nitrogen-doped porous carbon nanotubes with high-efficiency electrocatalysis for room-temperature sodium-sulfur batteries. *Nat. Commun.* **2019**, *10*, 4793. DOI PubMed PMC
47. Yang, W.; Yang, W.; Zou, R.; et al. Cellulose nanofiber-derived carbon aerogel for advanced room-temperature sodium-sulfur batteries. *Carbon. Energy.* **2022**, *5*, e203. DOI
48. Zhang, Y.; Guo, X.; Yang, Q.; et al. Chemical and spatial dual-confinement engineering for stable Na-S batteries with approximately 100% capacity retention. *Proc. Natl. Acad. Sci. U.S.A.* **2023**, *120*, e2314408120. DOI PubMed PMC
49. Du, W.; Xu, Q.; Zhan, R.; Zhang, Y.; Luo, Y.; Xu, M. Synthesis of hollow porous carbon microspheres and their application to room-temperature Na-S batteries. *Mater. Lett.* **2018**, *221*, 66-9. DOI
50. Ma, Q.; Du, G.; Guo, B.; et al. Carbon-wrapped cobalt nanoparticles on graphene aerogel for solid-state room-temperature sodium-sulfur batteries. *Chem. Eng. J.* **2020**, *388*, 124210. DOI
51. Guo, B.; Du, W.; Yang, T.; et al. Nickel hollow spheres concatenated by nitrogen-doped carbon fibers for enhancing electrochemical kinetics of sodium-sulfur batteries. *Adv. Sci.* **2019**, *7*, 1902617. DOI

52. Ye, C.; Jin, H.; Shan, J.; et al. A Mo_5N_6 electrocatalyst for efficient Na_2S electrodeposition in room-temperature sodium-sulfur batteries. *Nat. Commun.* **2021**, *12*, 7195. DOI
53. Hu, P.; Xiao, F.; Wu, Y.; et al. Covalent encapsulation of sulfur in a graphene/N-doped carbon host for enhanced sodium-sulfur batteries. *Chem. Eng. J.* **2022**, *443*, 136257. DOI
54. Tang, W.; Zhong, W.; Wu, Y.; et al. Vanadium carbide nanoparticles incorporation in carbon nanofibers for room-temperature sodium sulfur batteries: confining, trapping, and catalyzing. *Chem. Eng. J.* **2020**, *395*, 124978. DOI
55. Ye, C.; Jiao, Y.; Chao, D.; et al. Electron-state confinement of polysulfides for highly stable sodium-sulfur batteries. *Adv. Mater.* **2020**, *32*, 1907557. DOI
56. Du, W.; Wu, Y.; Yang, T.; et al. Rational construction of rGO/VO_2 nanoflowers as sulfur multifunctional hosts for room temperature Na-S batteries. *Chem. Eng. J.* **2020**, *379*, 122359. DOI
57. Lu, Q.; Wang, X.; Cao, J.; et al. Freestanding carbon fiber cloth/sulfur composites for flexible room-temperature sodium-sulfur batteries. *Energy. Storage. Mater.* **2017**, *8*, 77-84. DOI
58. Yang, Q.; Yang, T.; Gao, W.; et al. An MXene-based aerogel with cobalt nanoparticles as an efficient sulfur host for room-temperature Na-S batteries. *Inorg. Chem. Front.* **2020**, *7*, 4396-403. DOI
59. Yang, H.; Zhou, S.; Zhang, B. W.; et al. Architecting freestanding sulfur cathodes for superior room-temperature Na-S batteries. *Adv. Funct. Mater.* **2021**, *31*, 2102280. DOI